An InAs/high-*k*/low-*k* structure: Electron transport and interface analysis

Toshimasa Ui, Ryousuke Mori, Son Phuong Le, Yoshifumi Oshima, and Toshi-kazu Suzuki[a]
Center for Nano Materials and Technology, Japan Advanced Institute of Science and Technology (JAIST), 1-1 Asahidai, Nomi, Ishikawa 923-1292, Japan

(Received 23 January 2017; accepted 26 April 2017; published online 4 May 2017)

We fabricated and investigated an InAs/high-*k*/low-*k* structure in comparison with an InAs/low-*k* structure, where the former and the latter are respectively obtained by bonding of InAs/Al_2O_3/AlN and InAs on low-*k* flexible substrates (FS). The InAs/high-*k*/low-*k* (InAs/Al_2O_3/AlN/FS) exhibits electron mobilities immune to interface fluctuation scattering, whereas this scattering is serious for the InAs/low-*k* (InAs/FS). Moreover, we find that electron sheet concentrations in the InAs/high-*k*/low-*k* are significantly higher than those in the InAs/low-*k*. From InAs/Al_2O_3 interface analysis by energy-dispersive X-ray spectroscopy and electron energy-loss spectroscopy, we find that the higher electron concentrations can be attributed to natural modulation doping from Al_2O_3 to InAs. [http://dx.doi.org/10.1063/1.4983176]

I. INTRODUCTION

InAs is an important narrow-gap compound semiconductor,[1,2] applicable to mid-infrared optical devices,[3] high-performance field-effect transistors,[4–7] and also interband tunnel transistors.[8,9] In particular, heterogeneous integration of InAs devices on foreign host substrates is quite important.[10–13] We previously fabricated and investigated an InAs/low-*k* structure, where high-quality InAs thin films are bonded on host low-dielectric-constant (low-*k*) flexible substrates (FS),[14–17] by using epitaxial lift-off (ELO) and van der Waals bonding (VWB) method.[18,19] The InAs/low-*k* (InAs/FS) exhibits high electron mobilities, where the FS with $k \sim 3$, polyethylene terephthalate (PET) coated by bisazide-rubber, has a merit for device applications because of a low parasitic capacitance. However, we found a serious problem of InAs/FS interface fluctuation affecting electron mobilities[15] and low-frequency noise.[17] In addition, poor heat release capability due to a low thermal conductivity of PET, $\kappa \sim 0.3$ W/m-K, is also problematic.

Considering these problems, in this work, we fabricated and investigated an InAs/high-*k*/low-*k* structure, where a thin high-*k* insulator layer between InAs and the low-*k* FS can be beneficial to suppress the interface fluctuation and to improve the heat release capability, almost keeping the merit of the low parasitic capacitance of the FS. We employed Al_2O_3/AlN as a high-*k* insulator layer, where $k \sim 9$ and $\kappa \sim 30$ W/m-K for Al_2O_3, and $k \sim 9$ and $\kappa \sim 300$ W/m-K for AlN, to obtain the InAs/high-*k*/low-*k* (InAs/Al_2O_3/AlN/FS). Electron transport properties of the InAs/high-*k*/low-*k* were investigated in comparison with those of the InAs/low-*k*, for InAs film thicknesses from $\lesssim 10$ nm to ~ 150 nm. As a result, we find that the InAs/high-*k*/low-*k* exhibits electron mobilities immune to interface fluctuation scattering. We also find that electron sheet concentrations in the InAs/high-*k*/low-*k* are significantly higher than those in the InAs/low-*k*. Interface analysis by energy-dispersive X-ray spectroscopy (EDX) and electron energy-loss spectroscopy (EELS) for the InAs/Al_2O_3 interface

[a]Author to whom correspondence should be addressed; electronic mail: tosikazu@jaist.ac.jp

indicates that the higher electron concentrations can be attributed to natural modulation doping from Al_2O_3 to InAs.

II. SAMPLE FABRICATION

The InAs/high-*k*/low-*k* and InAs/low-*k* structures were fabricated as shown in the top of Fig. 1. Using a heterostructure, InAs device layer (500 nm thickness)/ AlAs sacrificial layer (4 nm thickness)/ InAs buffer layer (2500 nm thickness)/ GaAs(001), we carried out ELO,[14–17] separation of the InAs device layer attached to an adhesive sheet. The InAs device layer was transferred onto an intermediate support, a sapphire(0001) coated by resists, followed by removal of the adhesive sheet and InAs surface cleaning using phosphoric acid. For the InAs/high-*k*/low-*k* structure, high-*k* insulator deposition on the InAs was carried out; we deposited Al_2O_3 (50 nm thickness) by atomic layer deposition (ALD) using trimethylaluminum and H_2O, and AlN (30 nm thickness) by electron cyclotron resonance (ECR) sputtering deposition using an Ar-N_2 plasma and an AlN target. The InAs/Al_2O_3/AlN was separated from the intermediate support, followed by 'inverted' VWB on the low-*k* FS, PET coated by bisazide-rubber, to obtain the InAs/high-*k*/low-*k* (InAs/Al_2O_3/AlN/FS). The reasons of employing Al_2O_3/AlN as a high-*k* insulator layer are as follows. If we employ a single layer deposition of Al_2O_3 or AlN, we observe convex or concave sample warpage during VWB as shown in Fig. 2, probably owing to a strain during the deposition, which makes the process quite difficult. On the other hand, employing the Al_2O_3/AlN layer is advantageous to suppress sample warpage as shown in Fig. 2, owing to strain balancing, and consequently helpful for easiness of the VWB process. The thicknesses of Al_2O_3 and AlN are optimized; we found that, for the 50-nm-thick Al_2O_3, the 30-nm-thick AlN leads to an almost flat sample profile. In addition, the ALD deposition of Al_2O_3 on InAs is suitable to avoid interface fluctuations, while the ECR sputtering deposition of AlN causes damages of the InAs surface. Therefore, we employed the ALD deposition of Al_2O_3 followed by the ECR sputtering deposition of AlN to obtain the InAs/Al_2O_3/AlN. Moreover, in order to obtain the InAs/low-*k* (InAs/FS), the InAs without high-*k* insulator deposition was separated from the intermediate support, followed by the 'inverted' VWB on the low-*k* FS.

Using the InAs/high-*k*/low-*k* and the InAs/low-*k*, we obtained Hall-bar devices with current flowing direction [1$\bar{1}$0], by wet-etching isolation, Ohmic electrode formation, and channel thinning

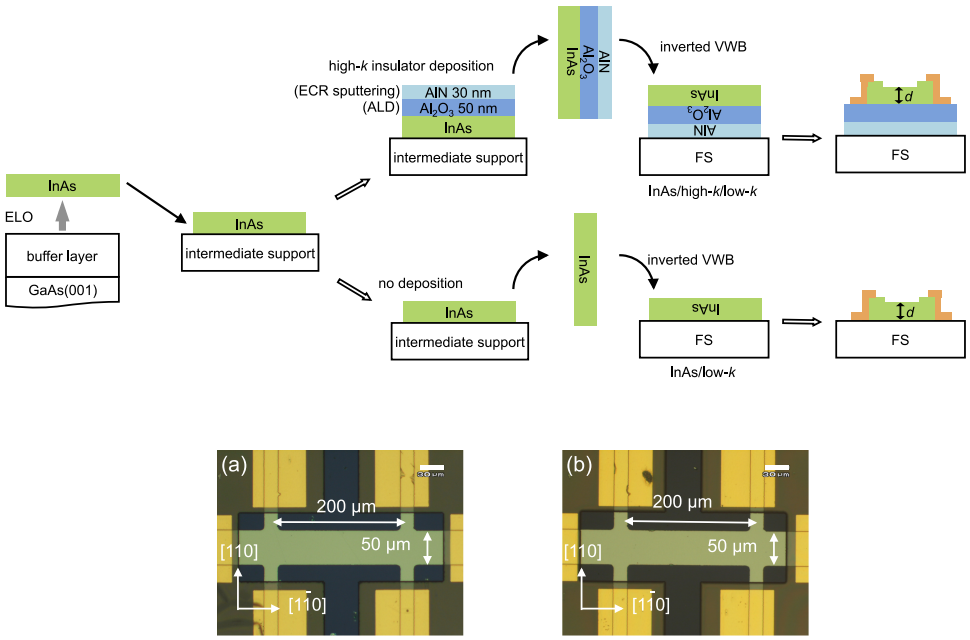

FIG. 1. (Top) Schematic fabrication process of the InAs/high-*k*/low-*k* (InAs/Al_2O_3/AlN/FS) and InAs/low-*k* (InAs/FS) structures. (Bottom) Nomarski optical microscope images of (a) InAs/high-*k*/low-*k* and (b) InAs/low-*k* Hall-bar devices with current flowing direction [1$\bar{1}$0].

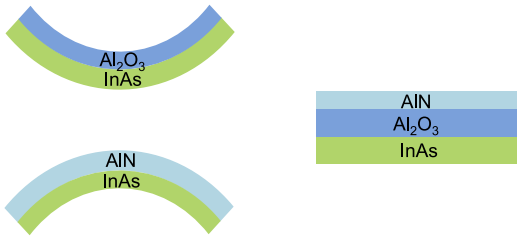

FIG. 2. (Left) Schematic warpage during VWB in the case of employing a single layer deposition of Al_2O_3 or AlN. (Right) Employing the Al_2O_3/AlN layer is advantageous to suppress warpage.

by wet etching.[14–17] Nomarski optical microscope images of the Hall-bar devices are shown in the bottom of Fig. 1, where the differential interference contrasts indicate same smooth surfaces for the InAs/high-k/low-k and the InAs/low-k. The Hall-bar devices enable us to characterize electron transport properties of the InAs/high-k/low-k and the InAs/low-k for several InAs channel thicknesses from $\lesssim 10$ nm to ~ 150 nm, where the 'inverted' VWB is advantageous to obtain a high crystal quality after the thinning according to the growth-direction dislocation distribution.[20]

III. ELECTRON TRANSPORT PROPERTIES

From room-temperature measurements of the Hall-bar devices, as shown in Fig. 3, we obtained electron mobilities μ and electron sheet concentrations n_s as functions of the InAs channel thickness d, where the error bars of d come from thickness measurements.[15] The InAs/low-k for $d \lesssim 15$ nm exhibits μ rapidly decreasing with decrease in d, $\mu \propto d^{\gamma}$ ($\gamma \simeq 5$-6) attributed to serious interface fluctuation scattering or thickness fluctuation scattering;[15,21–26] when there is a bonding interface fluctuation, the confinement potential fluctuates with a thickness fluctuation in the Cartesian coordinate, leading to $\mu \propto d^{\gamma}$ behavior. On the other hand, for the InAs/high-k/low-k, we do not observe $\mu \propto d^{\gamma}$ behavior,

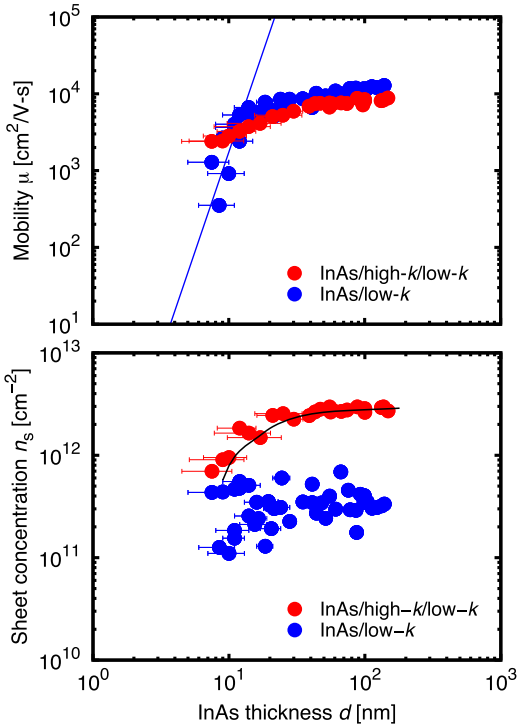

FIG. 3. Electron mobilities μ and electron sheet concentrations n_s as functions of the InAs channel thickness d for the InAs/high-k/low-k and InAs/low-k structures. The blue solid line for μ shows $\mu \propto d^{\gamma}$ ($\gamma \simeq 5.2$). The black solid curve for n_s is obtained by Poisson-Schrödinger calculation.

indicating that the InAs/high-k/low-k exhibits μ immune to interface fluctuation scattering even for $d \lesssim 10$ nm. This can be attributed to the fact that the interface fluctuation of the InAs/Al_2O_3 obtained by ALD is smaller than that of the InAs/FS obtained by VWB. The InAs/low-k for $d \gtrsim 15$ nm exhibits μ dominated by Coulomb scattering, where μ slowly decreases with decrease in d.[15] The InAs/high-k/low-k exhibits similar μ attributed to Coulomb scattering, but slightly lower than that of the InAs/low-k. This suggests more Coulomb scattering centers near the interface for the InAs/high-k/low-k, as discussed later. We also find that n_s in the InAs/high-k/low-k is significantly higher (10^{12} cm^{-2} order) with a smaller dispersion than in the InAs/low-k (10^{11} cm^{-2} order). The observed higher n_s with the smaller dispersion suggests that electrons are supplied from Al_2O_3 to InAs through the InAs/Al_2O_3 interface.

IV. INTERFACE ANALYSIS

In order to examine the possibility of the electron supply from Al_2O_3 to InAs, we carried out InAs/Al_2O_3 interface analysis by using a scanning transmission electron microscope (STEM) with an acceleration voltage of 120 kV. Figure 4(a) shows a high angle annular dark field (HAADF) STEM image near the InAs/Al_2O_3 interface, where the STEM sample thickness is around 50 nm or less, and the origin of the position x defined later corresponds to the interface. EDX maps for In-Lα, As-L, Al-Kα, and O-Kα near the InAs/Al_2O_3 interface were obtained in the STEM as shown in Fig. 4(b). EDX intensities (integrated along y direction parallel to the interface and normalized) as functions

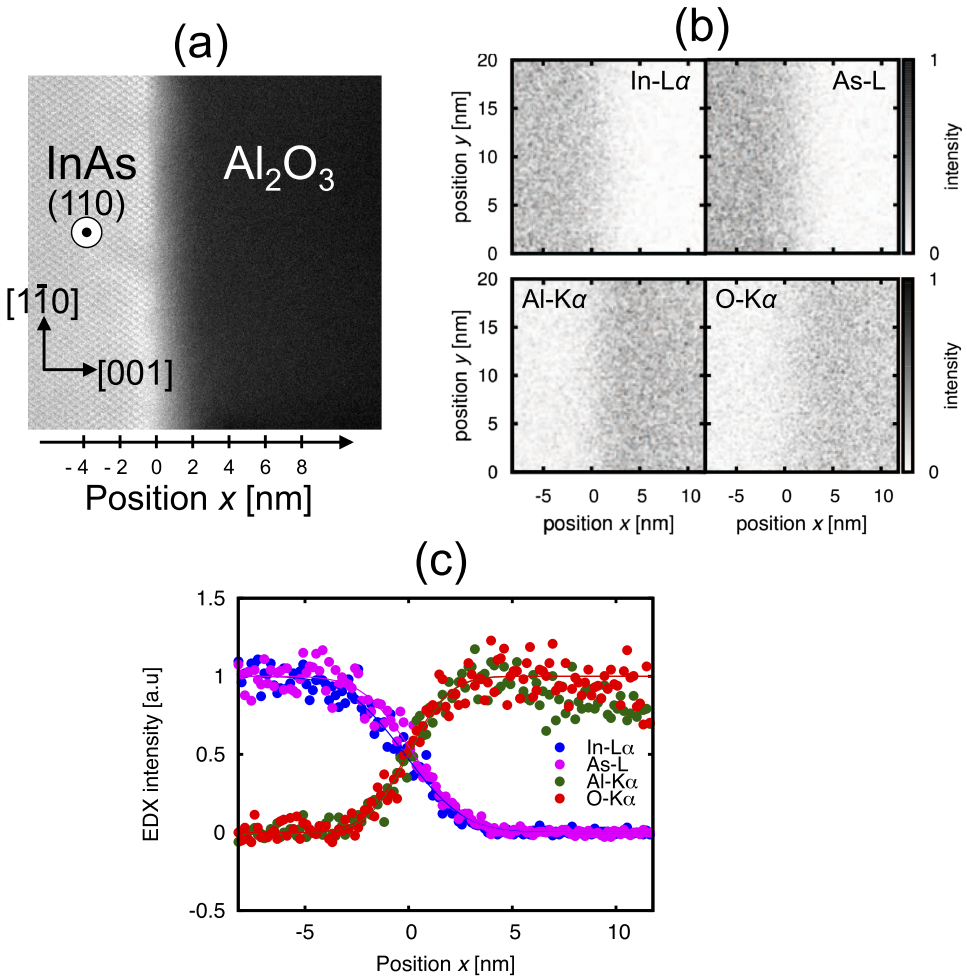

FIG. 4. (a) A HAADF STEM image near the InAs/Al_2O_3 interface. (b) EDX maps obtained in STEM for In-Lα, As-L, Al-Kα, and O-Kα near the InAs/Al_2O_3 interface. (c) EDX intensities as functions of the position x.

of the position x are shown in Fig. 4(c). with fitting curves. The fitting curves are given by the error function, $[1-\mathrm{erf}[(x-x_0)/\sqrt{2}\sigma]]/2$ (for In-Lα and As-L) or $[1+\mathrm{erf}[(x-x_0)/\sqrt{2}\sigma]]/2$ (for Al-Kα and O-Kα), with $x_0 = 0$ for O-Kα as the definition of the origin corresponding to the interface position, and $x_0 \simeq 0$ for In-Lα, As-L, and Al-Kα.

Moreover, in the STEM, we carried out EELS near the InAs/Al_2O_3 interface. Figure 5 shows EELS spectra around the O-K edge for x = −1.5-+3.5 nm. While clear O-K edge peaks at 541 eV are observed for positive x, clear satellite peaks at 532 eV are observed only for $x \gtrsim 1.5$ nm. Figure 6 shows (a) O-K edge peak and (b) satellite peak intensities as functions of the position x, which can be also fitted by $[1+\mathrm{erf}[(x-x_0)/\sqrt{2}\sigma]]/2$ using the error function. For comparison, the EDX O-Kα intensity is also shown. We find the onset position $x_0 \simeq 0$ for the O-K edge peak, which is consistent with the EDX O-Kα intensity, while $x_0 \simeq 1.3$ nm for the satellite peak. In Al_2O_3, there are inevitable oxygen-vacancies, which act as donors.[27,28] It has been reported that, non-ionized oxygen-vacancy donors (occupied by electrons) in Al_2O_3 can cause the satellite peak, while ionized oxygen-vacancy donors (unoccupied by electrons) do not give the satellite peak.[29] Therefore, we conclude that oxygen-vacancy donors are ionized near the InAs/Al_2O_3 interface ($x \lesssim 1.3$ nm), while not ionized for the Al_2O_3-inside ($x \gtrsim 1.3$ nm). This indicates that natural modulation doping takes place at the InAs/Al_2O_3 interface; oxygen-vacancy donors near the interface supply electrons from Al_2O_3 to InAs leading to the higher n_s, and become ionized donors. The ionized donors act as Coulomb scattering centers near the interface, giving the slightly lower μ. The situation is similar to the natural modulation doping taking place at InAs/AlSb interfaces,[30,31] where deep donors due to antisite defects in AlSb supply electrons from AlSb to InAs, leading to a high electron concentration in InAs.

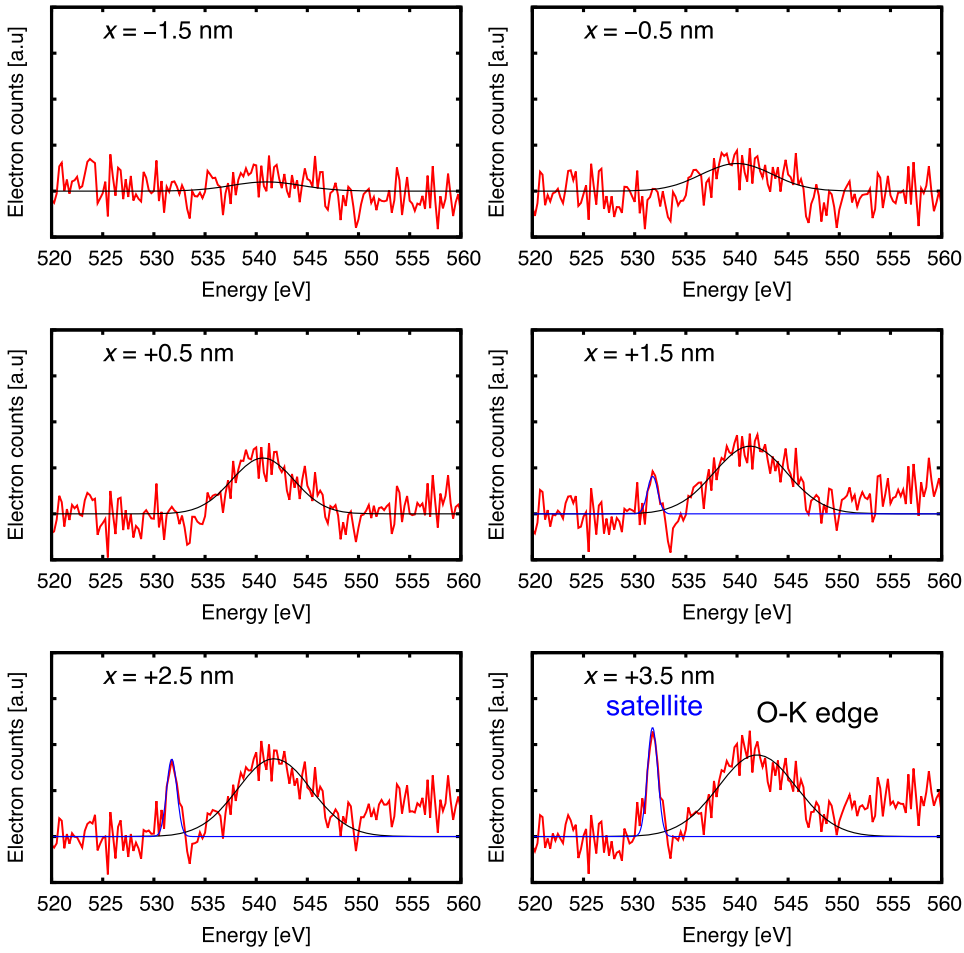

FIG. 5. EELS spectra for x = −1.5-+3.5 nm, showing O-K edge peaks at 541 eV and satellite peaks at 532 eV.

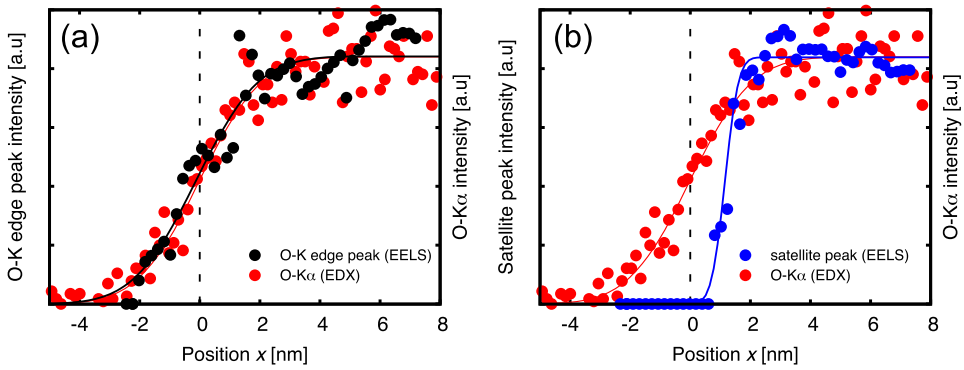

FIG. 6. (a) O-K edge peak and (b) satellite peak intensities as functions of the position x, with the EDX O-Kα intensity.

V. POISSON-SCHRÖDINGER CALCULATION

In order to confirm the natural modulation doping picture quantitatively, we carried out Poisson-Schrödinger calculation.[32] Figure 7 shows examples of the calculated energy band profile and electron distribution at 300 K, where we plot the conduction band bottom energy E_c, the valence band top energy E_v, the oxygen-vacancy donor level E_D, the Fermi energy E_F, and the electron concentration ρ

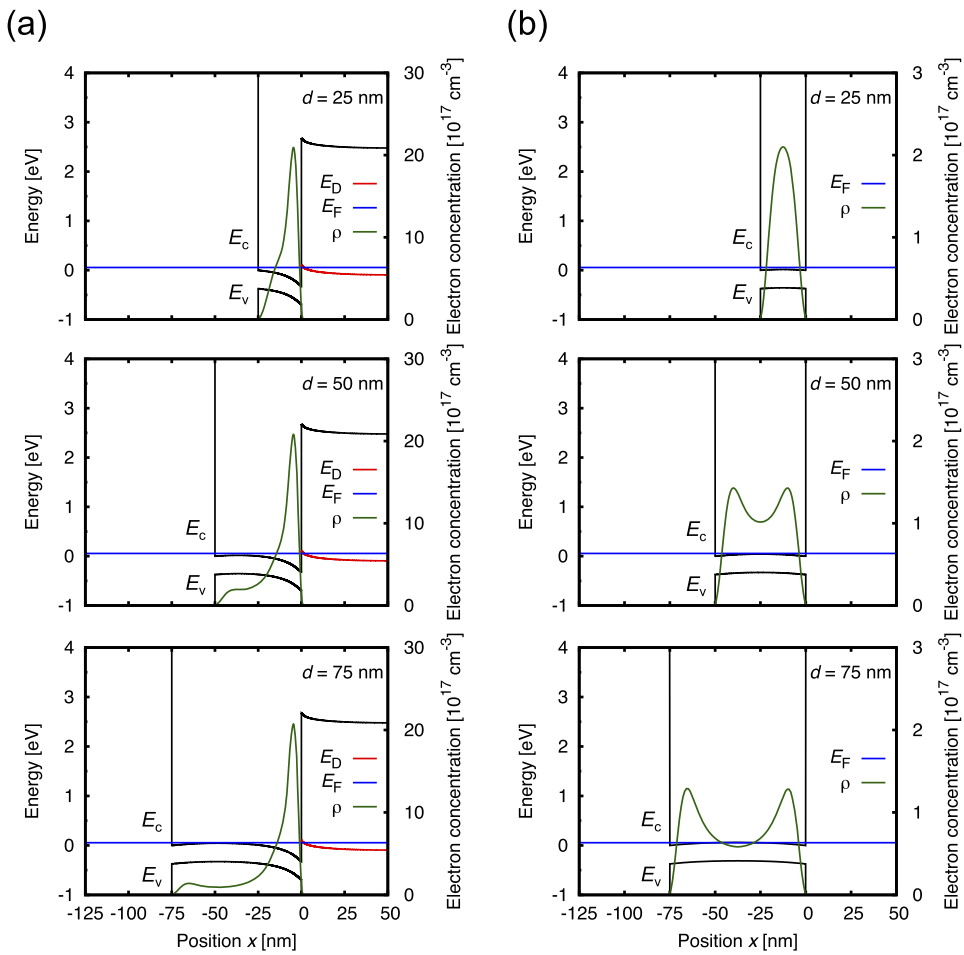

FIG. 7. Examples of the calculated energy band profile and electron distribution at 300 K for (a) InAs/Al_2O_3 and (b) InAs/FS, showing the conduction band bottom energy E_c, the valence band top energy E_v, the oxygen-vacancy donor level E_D, the Fermi energy E_F, and the electron concentration ρ (in the unit of cm^{-3}).

(in the unit of cm^{-3}), for (a) InAs/Al_2O_3 and (b) InAs/FS modeled as free-standing InAs. The energy gaps of Al_2O_3 and InAs are set to be 6.8 eV and 0.37 eV, respectively, with the conduction band offset of 3.0 eV.[33,34] We employ Fermi level pinning at the InAs surface $E_F - E_c = 56$ meV, giving 10^{11} cm^{-2} order electron sheet concentrations for the InAs/FS. As shown in Fig. 7(a), we observe an electron accumulation in InAs near the InAs/Al_2O_3 interface, and a depletion region in Al_2O_3. We obtain a depletion length in Al_2O_3 $x_{dep} \simeq 1.3$ nm in good agreement with the EELS result, assuming 1.6×10^{19} cm^{-3} oxygen-vacancy donors in Al_2O_3 with a level of $E_c - E_D = 2.6$ eV, located ~ 4 eV above the valence band top.[35] Moreover, from the calculation, we obtain n_s as a function of d for the InAs/Al_2O_3, as shown in the black solid curve of Fig. 3. We find good agreement between the calculated and experimental results, which supports the natural modulation doping picture.

VI. SUMMARY

In summary, we investigated the InAs/high-*k*/low-*k* (InAs/Al_2O_3/AlN/FS) in comparison with the InAs/low-*k* (InAs/FS). While interface fluctuation scattering is serious for the InAs/low-*k*, we find that the InAs/high-*k*/low-*k* exhibits electron mobilities immune to this scattering, attributed to small InAs/Al_2O_3 interface fluctuation obtained by ALD. We also find higher electron sheet concentrations in the InAs/high-*k*/low-*k* than in the InAs/low-*k*. From EDX and EELS, we conclude that natural modulation doping takes place at the InAs/Al_2O_3 interface leading to the higher electron concentrations, as supported by Poisson-Schrödinger calculation.

ACKNOWLEDGMENTS

This work was supported by JSPS KAKENHI Grant Number 26249046, 15K13348. We would like to thank K. Higashimine for helpful discussions.

[1] A. Milnes and A. Polyakov, Mater. Sci. Eng. B **18**, 237 (1993).
[2] H. Kroemer, Physica E **20**, 196 (2004).
[3] Z. Yin and X. Tang, Solid-State Electron. **51**, 6 (2007).
[4] B. R. Bennett, R. Magno, J. B. Boos, W. Kruppa, and M. G. Ancona, Solid-State Electron. **49**, 1875 (2005).
[5] D.-H. Kim and J. del Alamo, IEEE Electron Device Lett. **31**, 806 (2010).
[6] N. Li, E. S. Harmon, J. Hyland, D. B. Salzman, T. P. Ma, Y. Xuan, and P. D. Ye, Appl. Phys. Lett. **92**, 143507 (2008).
[7] S. H. Kim, M. Yokoyama, R. Nakane, O. Ichikawa, T. Osada, M. Hata, M. Takenaka, and S. Takagi, IEEE Trans. Electron Devices **61**, 1354 (2014).
[8] Q. Zhang, W. Zhao, and A. Seabaugh, IEEE Electron Device Lett. **27**, 297 (2006).
[9] M. Luisier and G. Klimeck, IEEE Electron Device Lett. **30**, 602 (2009).
[10] H. Ko, K. Takei, R. Kapadia, S. Chuang, H. Fang, P. W. Leu, K. Ganapathi, E. Plis, H. S. Kim, S.-Y. Chen, M. Madsen, A. C. Ford, Y.-L. Chueh, S. Krishna, S. Salahuddin, and A. Javey, Nature **468**, 286 (2010).
[11] K. Takei, S. Chuang, H. Fang, R. Kapadia, C.-H. Liu, J. Nah, H. S. Kim, E. Plis, S. Krishna, Y.-L. Chueh, and A. Javey, Appl. Phys. Lett. **99**, 103507 (2011).
[12] K. Takei, H. Fang, S. B. Kumar, R. Kapadia, Q. Gao, M. Madsen, H. S. Kim, C.-H. Liu, Y.-L. Chueh, E. Plis, S. Krishna, H. A. Bechtel, J. Guo, and A. Javey, Nano Lett. **11**, 5008 (2011).
[13] H. Schmid, M. Borg, K. Moselund, L. Gignac, C. M. Breslin, J. Bruley, D. Cutaia, and H. Riel, Appl. Phys. Lett. **106**, 233101 (2015).
[14] H. Takita, N. Hashimoto, C. T. Nguyen, M. Kudo, M. Akabori, and T. Suzuki, Appl. Phys. Lett. **97**, 012102 (2010).
[15] C. T. Nguyen, H.-A. Shih, M. Akabori, and T. Suzuki, Appl. Phys. Lett. **100**, 232103 (2012).
[16] T. Suzuki, H. Takita, C. T. Nguyen, and K. Iiyama, AIP Advances **2**, 042105 (2012).
[17] S. P. Le, T. Ui, and T. Suzuki, Appl. Phys. Lett. **107**, 192103 (2015).
[18] Y. Jeong, M. Shindo, M. Akabori, and T. Suzuki, Appl. Phys. Express **1**, 021201 (2008).
[19] Y. Jeong, M. Shindo, H. Takita, M. Akabori, and T. Suzuki, Phys. Stat. Sol. C **5**, 2787 (2008).
[20] Y. Jeong, H. Choi, and T. Suzuki, J. Cryst. Growth **301-302**, 235 (2007).
[21] A. Gold, Solid State Commun. **60**, 531 (1986).
[22] A. Gold, Phys. Rev. B **35**, 723 (1987).
[23] H. Sakaki, T. Noda, K. Hirakawa, M. Tanaka, and T. Matsusue, Appl. Phys. Lett. **51**, 1934 (1987).
[24] C. R. Bolognesi, H. Kroemer, and J. H. English, Appl. Phys. Lett. **61**, 213 (1992).
[25] T. Ishihara, K. Uchida, J. Koga, and S. Takagi, Jpn. J. Appl. Phys. **45**, 3125 (2006).
[26] A. Gold, J. Appl. Phys. **103**, 043718 (2008).
[27] J. R. Weber, A. Janotti, and C. G. Van de Walle, J. Appl. Phys. **109**, 033715 (2011).
[28] M. Choi, A. Janotti, and C. G. Van de Walle, J. Appl. Phys. **113**, 044501 (2013).
[29] S. Nigo, M. Kubota, Y. Harada, T. Hirayama, S. Kato, H. Kitazawa, and G. Kido, J. Appl. Phys. **112**, 033711 (2012).
[30] J. Shen, J. D. Dow, S. Y. Ren, S. Tehrani, and H. Goronkin, J. Appl. Phys. **73**, 8313 (1993).
[31] J. Shen, H. Goronkin, J. D. Dow, and S. Y. Ren, J. Appl. Phys. **77**, 1576 (1995).

[32] G. L. Snider, *Computer Program 1D Poisson/Schrödinger: A Band Diagram Calculator*(University of Notre Dame, Notre Dame, Indiana, 1995).
[33] Q. Zhang, R. Li, R. Yan, T. Kosel, H. G. Xing, A. C. Seabaugh, K. Xu, O. A. Kirillov, D. J. Gundlach, C. A. Richter, and N. V. Nguyen, Appl. Phys. Lett. **102**, 012101 (2013).
[34] W. Li, Q. Zhang, R. Bijesh, O. A. Kirillov, Y. Liang, I. Levin, L.-M. Peng, C. A. Richter, X. Liang, S. Datta, D. J. Gundlach, and N. V. Nguyen, Appl. Phys. Lett. **105**, 213501 (2014).
[35] M. Y. Yang, K. Kamiya, B. Magyari-Köpe, M. Niwa, Y. Nishi, and K. Shiraishi, Appl. Phys. Lett. **103**, 093504 (2013).